mathematics

Article

Optimal Design of Group Orthogonal Phase-Coded Waveforms for MIMO Radar

Tianqu Liu [1], Jinping Sun [1], Guohua Wang [2], Xianxun Yao [1,*] and Yaqiong Qiao [1]

[1] School of Electronic and Information Engineering, Beihang University, Beijing 100191, China; tqliu@buaa.edu.cn (T.L.); sunjinping@buaa.edu.cn (J.S.); qiaoyaqiong@crscd.com.cn (Y.Q.)
[2] Hertzwell Pte Ltd., Singapore 138565, Singapore; wghwood@hotmail.com
* Correspondence: xianxun.yao@buaa.edu.cn; Tel.: +86-010-8231-7240

Abstract: Digital radio frequency memory (DRFM) has emerged as an advanced technique to achieve a range of jamming signals, due to its capability to intercept waveforms within a short time. multiple-input multiple-output (MIMO) radars can transmit agile orthogonal waveform sets for different pulses to combat DRFM-based jamming, where any two groups of waveform sets are also orthogonal. In this article, a group orthogonal waveform optimal design model is formulated in order to combat DRFM-based jamming by flexibly designing waveforms for MIMO radars. Aiming at balancing the intra- and intergroup orthogonal performances, the objective function is defined as the weighted sum of the intra- and intergroup orthogonal performance metrics. To solve the formulated model, in this article, a group orthogonal waveform design algorithm is proposed. Based on a primal-dual-type method and proper relaxations, the proposed algorithm transforms the original problem into a series of simple subproblems. Numerical results demonstrate that the obtained group orthogonal waveforms have the ability to flexibly suppress DRFM-based deceptive jamming, which is not achievable using p-majorization–minimization (p-MM) and primal-dual, two of the most advanced orthogonal waveform design algorithms.

Keywords: waveform design; optimization; MIMO radar; group orthogonal; phase-coded; radar countermeasures

MSC: 90C26

Citation: Liu, T.; Sun, J.; Wang, G.; Yao, X.; Qiao, Y. Optimal Design of Group Orthogonal Phase-Coded Waveforms for MIMO Radar. *Mathematics* **2024**, *12*, 903. https://doi.org/10.3390/math12060903

Academic Editor: Alessandro Niccolai

Received: 10 January 2024
Revised: 5 March 2024
Accepted: 16 March 2024
Published: 19 March 2024

1. Introduction

Waveform diversity and multiantenna technologies are utilized in multiple-input multiple-output (MIMO) radars to improve their angular resolution, antijamming ability, and other target detection abilities [1–4]. By transmitting orthogonal waveform sets, an MIMO radar can separate the received waveforms transmitted by different antennas. Generally, an MIMO radar uses a matched filter bank to process the echoes. Thus, the cross-correlation functions among the orthogonal waveforms should be as low as possible. Meanwhile, in order to achieve a good pulse compression performance, the autocorrelation functions' side-lobes should also be as low as possible.

Designing multiple different phase-coding sequences with a low cross-correlation is one of the most common ways to realize an orthogonal waveform set [5–7]. With a large number of transmitted waveforms, a phase-coded waveform set is difficult to intercept by traditional jammers [8]. Integrated side-lobe level (ISL) and peak side-lobe level (PSL) are two commonly used metrics for orthogonal MIMO radar phase-coded waveform sets [9–11]. Aiming to minimize the ISL, multicyclic-algorithm-new (multi-CAN [12]), majorization–minimization correlation (MM-Corr [13]), ISL-New [14], alternating-direction-method-of-multipliers (ADMM [15]), etc., algorithms have been proposed, although they cannot minimize the PSL. PSL minimization is more complex and harder than ISL minimization. Thus far, some researchers have proposed effective PSL optimization algorithms [16–20], with the method based on primal-dual achieving the best performance [18]. Particularly, the p-MM algorithm can obtain almost the same PSL metrics as primal-dual, with much lower ISL metrics [19]. All the abovementioned ISL and PSL optimization algorithms lead to a single set of orthogonal waveforms. With a well-designed orthogonal phase-coded waveform set, the MIMO radar achieves a high waveform diversity gain and a low probability of intercept.

With the advent of digital radio frequency memory (DRFM) [21,22], more advanced jamming technologies have been rapidly developed. DRFM-based jammers pose a great threat to MIMO radar, and can perform read and copy functions and diverse parameter modulations (like delay, Doppler, etc.) within a short time. Therefore, DRFM-based jammers may seriously affect the operational capabilities of MIMO radars in the future.

The transmitting agile waveform is an effective way to combat modern DRFM-based jamming [23,24]. Although DRFM-based jammers have a strong ability to intercept waveforms, they must delay at least one pulse repetition time (PRT) to complete jamming signal generation. If the correlation between adjacent pulses is low, it is difficult for the DRFM-based jammers to interfere with the waveforms. From the perspective of orthogonality, MIMO radars should transmit an orthogonal waveform set within each pulse. In different pulse intervals, the waveform sets should also be orthogonal to each other. Thus, even though the jammers have intercepted the waveforms in the previous pulse, they cannot interfere with the subsequent pulses. Therefore, in this article, the MIMO radar antijamming agile waveform is modeled as multiple groups of orthogonal waveform sets. The abovementioned PSL and ISL optimization algorithms can be used to design all groups of waveforms directly. However, they cannot finely control the intra- and intergroup orthogonal performance.

In order to balance the intra- and intergroup orthogonal performances, in this article, an optimization model for designing group orthogonal waveforms is proposed, which is able to maximize the waveform diversity gain when diverse DRFM-based jamming signals are encountered. The proposed model can overcome the shortcomings of existing methods. Considering that target detection is based on correlation peak detection, in the proposed model, the objective function is formulated considering the following two aspects. The first is to minimize the cross-correlation peak and autocorrelation side-lobe peaks within each group of orthogonal waveforms, which can be evaluated by the traditional PSL metric. The second is to minimize the cross-correlation peak among different groups of orthogonal waveforms, which can be evaluated by the peak cross-correlation level (PCL) metric. The objective function of the proposed model is the weighted sum of the PSL and PCL metrics. These metrics evaluate the MIMO waveform diversity gain and jamming suppression performance, respectively.

In order to solve the proposed optimization model, in this article, a group orthogonal waveform optimal design algorithm is proposed. Minimizing the correlation function peak in the proposed model is difficult. Based on some relaxations, ref. [18] divided the origin PSL minimization problem into a series of convex subproblems. Inspired by the relaxation approach in [18], in this article, the intra- and intergroup correlation functions are processed separately and the proposed optimization model is transformed into a series of solvable subproblems. Finally, the proposed algorithm generates solutions to each subproblem. The numerical results show that the proposed algorithm can effectively design multiple groups of orthogonal waveform sets. The cross-correlation functions between the waveform sets are also low. The antijamming simulation results demonstrate that the designed group orthogonal waveforms can balance the DRFM-based deceptive jamming suppression and range compression performances of MIMO radar by adjusting the weighting factors.

2. Problem Formulation

The optimization variables in group orthogonal waveform design are G groups of waveforms, with each group consisting of M waveforms. Considering phase-coded waveform design, group orthogonal waveforms with intra- and intergroup orthogonality can be realized by assigning different waveforms with different phase-coded sequences. Since the pulse length, chip length, carrier frequency, and other radar system parameters have little effect on the correlation function side-lobe level, in this article, the group orthogonal waveforms $\{\mathbf{x}_i\}_{i=1}^{GM}$ are modeled as

$$x_i[n] = \exp(\mathrm{j}\varphi_{i,n}), i = 1, 2, \ldots, GM, n = 1, 2, \ldots, N \tag{1}$$

where N is the sequence length. The phase value continuously satisfies $\varphi_{i,n} \in [-\pi, \pi)$. The correlation functions of $\{\mathbf{x}_i\}_{i=1}^{GM}$ are defined as

$$r_{ij}[k] = \sum_{n=1}^{N} x_i[n+k]\overline{x}_j[n], k = -N+1, \ldots, N-1 \tag{2}$$

where $r_{ij}[k]$ is the auto- or cross-correlation function and $\overline{(\cdot)}$ represents the complex conjugate. The set of the indexes of intra- and intergroup correlation functions is defined as $\{i, j, k | i, j = 1, 2, \ldots, GM, k = -N+1, \ldots, N-1\}$.

To evaluate the group orthogonal waveforms' correlation properties, we consider the intra- and intergroup correlation functions separately. We use the traditional peak side-lobe level (PSL) metric [9–11] to evaluate the waveforms within each group. The PSL metric for the g-th group is defined as

$$\mathrm{PSL}_g \triangleq \frac{1}{N^2} \max_{(i,j,k)\in\mathcal{K}_g} \left| r_{ij}[k] \right|^2, g = 1, 2, \ldots, G \tag{3}$$

$$\mathcal{K}_g = \{i, j, k | i, j \in [M(g-1)+1,\ Mg], i \neq j \text{ or } k \neq 0\} \tag{4}$$

where set $\mathcal{K}_g$ contains the correlation function indexes within the g-th group of waveforms, except for the indexes of the autocorrelation peak values that are equal to N. Because there are only cross-correlation functions between different groups of waveforms, the following peak cross-correlation level (PCL) is defined to evaluate the intergroup cross-correlation peak.

$$\mathrm{PCL} \triangleq \frac{1}{N^2} \max_{(i,j,k)\in\mathcal{G}} \left| r_{ij}[k] \right|^2 \tag{5}$$

$$\mathcal{G} = \left\{ i, j, k \middle| (i, j, k) \notin \cup_{g=1}^{G} \mathcal{K}_g, i \neq j \right\} \tag{6}$$

The set $\mathcal{G}$ in Equation (6) contains all the indexes of intergroup cross-correlation functions.

The object of group orthogonal waveform design is to minimize the PSL_1, PSL_2,…, PSL_G and PCL metrics, which are functions of the optimization variables $\{\mathbf{x}_i\}_{i=1}^{GM}$. Thus, the optimization model can be expressed as

$$\begin{array}{ll} \min & \mathbf{f}(\{\mathbf{x}_i\}_{i=1}^{GM}) = (\mathrm{PSL}_1, \mathrm{PSL}_2, \cdots, \mathrm{PSL}_G, \mathrm{PCL}) \\ \text{s.t.} & |x_i[n]| = 1, \quad i = 1, 2, \ldots, GM,\ n = 1, 2, \ldots, N \end{array} \tag{7}$$

where $\mathbf{f}$ represents the objective function vector, which contains the convolution and $\max(\cdot)$ operations. In addition, the waveforms $\{\mathbf{x}_i\}_{i=1}^{GM}$ have constant modulus constraints. The optimization model (7) is a complex minimax problem with nonconvex constraints. In order to simplify problem (7), we introduce the variables ε_1, ε_2,…, ε_G and γ to constrain the PSL_1, PSL_2,…, PSL_G and PCL metrics values, respectively. Meanwhile, in order to balance the intra- and intergroup orthogonal performances, we introduce a weighting factor w, thereby transforming the original problem into the following single-objective problem.

$$
\begin{aligned}
&\min w \cdot \left(\textstyle\sum_{g=1}^{G} \varepsilon_g^2/G\right) + (1-w)\cdot\gamma^2 \\
&\text{s.t. } \varepsilon_g \geq \left|r_{ij}[k]\right|^2/N^2, \forall(i,j,k) \in \mathcal{K}_g, g = 1,2,\ldots,G \\
&\quad \gamma \geq \left|r_{ij}[k]\right|^2/N^2, \forall(i,j,k) \in \mathcal{G} \\
&\quad r_{ij}(k) = \textstyle\sum_n x_i[n+k]\overline{x}_j[n], \forall(i,j,k) \\
&\quad |x_i[n]| = 1, \forall(i,n)
\end{aligned}
\tag{8}
$$

Note that the convolution operations and constant modulus constraints in problem (8) are not conducive to solving this problem. Inspired by ref. [18], we introduced the auxiliary variables $\{\mathbf{h}_i\}_{i=1}^{GM}$ and $\rho_{ij}(k)$ to decompose the complex nonlinear convolutions. Then, the correlation function constraints are replaced by the following linear equality constraints:

$$
\begin{cases}
\rho_{ij}(k) = \sum_n x_i[n+k]\overline{h}_j[n], \forall(i,j,k) \\
\mathbf{h}_i^H\mathbf{x}_i = N, \|\mathbf{h}_i\|_2^2 \leq N, \forall i
\end{cases}
\tag{9}
$$

In Equation (9), if $\mathbf{h}_i = \mathbf{x}_i$ holds for all i = 1, 2,. . ., GM, then $\rho_{ij}(k)$ is equal to the correlation functions $r_{ij}(k)$. This equivalent constraint condition in Equation (9) is correct according to the proposition below.

Proposition 1. *The constraints* $\mathbf{h}_i^H\mathbf{x}_i = N,\ \|\mathbf{h}_i\|_2^2 \leq N$ *are equivalent to the constraint* $\mathbf{h}_i = \mathbf{x}_i$ *for all* i = 1, 2,. . ., GM.

Proof of Proposition 1. According to the Cauchy–Schwartz inequality,

$$
\mathbf{h}_i^H\mathbf{x}_i = N = \left|\mathbf{h}_i^H\mathbf{x}_i\right| \leq \|\mathbf{h}_i\|_2\|\mathbf{x}_i\|_2 = \sqrt{N}\|\mathbf{h}_i\|_2 \tag{10}
$$

If $\|\mathbf{h}_i\|_2 \leq \sqrt{N}$ holds, then inequality (10) implies $\|\mathbf{h}_i\|_2 = \sqrt{N}$. Using the equality condition of the Cauchy–Schwartz inequality, we obtain

$$
\mathbf{x}_i = \kappa\mathbf{h}_i, \kappa \in \mathbb{C} \tag{11}
$$

According to Equation (11) and $\mathbf{h}_i^H\mathbf{x}_i = N$, it is not difficult to find $\kappa = 1$. Thus, $\mathbf{h}_i = \mathbf{x}_i$ is obtained and the proof is complete. □

By introducing the variables $\{\mathbf{h}_i\}_{i=1}^{GM}$ and $\rho_{ij}(k)$, the nonlinear constraints are relaxed to linear convex constraints. However, the constant modulus constraints of $\{\mathbf{x}_i\}_{i=1}^{GM}$ in problem (8) are still coupled with its other constraints, which leads to difficulties in solving for $\{\mathbf{x}_i\}_{i=1}^{GM}$. Therefore, we introduce the variables $\{\mathbf{y}_i\}_{i=1}^{GM}$ to simplify the subproblem regarding $\{\mathbf{x}_i\}_{i=1}^{GM}$. The following conditions are added to ensure the obtained waveforms have a constant modulus.

$$
x_i[n] = y_i[n],\ |y_i[n]| = 1,\ \forall(i,n) \tag{12}
$$

Then, the constant modulus constraints are transferred to the subproblem regarding $\{\mathbf{y}_i\}_{i=1}^{GM}$, which is easy to solve, even with constant modulus constraints. The subproblem regarding $\{\mathbf{x}_i\}_{i=1}^{GM}$ becomes an unconstrained convex problem.

After introducing series auxiliary variables into the optimization model (8), we formulate the following group orthogonal waveform optimal design model:

$$
\begin{array}{ll}
\min & w \cdot \left(\sum_{g=1}^{G} \varepsilon_g^2 / G\right) + (1-w) \cdot \gamma^2 \\
\text{s.t.} & \left|\rho_{ij}(k)\right| \le \varepsilon_g, \forall (i,j,k) \in \mathcal{K}_g, g = 1,2,\ldots,G \\
& \left|\rho_{ij}(k)\right| \le \gamma, \forall (i,j,k) \in \mathcal{G} \\
& \rho_{ij}(k) = \sum_n x_i[n+k]\overline{h}_j[n], \forall (i,j,k) \\
& \mathbf{h}_i^H \mathbf{x}_i = N, \|\mathbf{h}_i\|_2^2 \le N, \forall i \\
& x_i[n] = y_i[n], |y_i[n]| = 1, \forall (i,n)
\end{array}
\tag{13}
$$

The weighting factor w can balance the intra- and intergroup correlation peak values. The optimization variables include $\{\mathbf{x}_i\}_{i=1}^{GM}$, $\{\mathbf{y}_i\}_{i=1}^{GM}$, $\{\mathbf{h}_i\}_{i=1}^{GM}$, $\rho_{ij}(k)$, γ, and ε_g, g = 1, 2,. . ., G. Although the dimensions of the optimization variables increase, the intractable nonlinear and nonconvex constraints in the optimization model (8) are relaxed into a series of linear and convex constraints.

3. Proposed Group Orthogonal Waveform Design Algorithm

Based on the characteristics of the objective function and the constraints in the optimization model (13), we formulated an augmented Lagrange function [25] and transformed problem (13) into the following constrained minimization problem:

$$
\begin{array}{ll}
\min & L\left(\varepsilon_1, \ldots, \varepsilon_G, \gamma, \left\{\rho_{ij}(k)\right\}, \{\mathbf{x}_i\}, \{\mathbf{y}_i\}, \{\mathbf{h}_i\}, \{\lambda_i\}, \left\{\alpha_{ijk}\right\}, \{\beta_{in}\}\right) \\
\text{s.t.} & \left|\rho_{ij}(k)\right| \le \varepsilon_g, \forall (i,j,k) \in \mathcal{K}_g, g = 1,2,\ldots,G \\
& \left|\rho_{ij}(k)\right| \le \gamma, \forall (i,j,k) \in \mathcal{G} \\
& \|\mathbf{h}_i\|_2^2 \le N, \forall i \\
& |y_i[n]| = 1, \forall (i,n)
\end{array}
\tag{14}
$$

The augmented Lagrange function L can be expressed as follows:

$$
\begin{array}{l}
L = w \cdot \left(\sum_{g=1}^{G} \varepsilon_g^2 / G\right) + (1-w) \cdot \gamma^2 + \mathrm{Re}\left[\sum_i \overline{\lambda}_i \left(\mathbf{h}_i^H \mathbf{x}_i - N\right)\right] \\
+\mathrm{Re}\left[\sum_{(i,j,k)\in(\cup_{g=1}^{G}\mathcal{K}_g)\cup\mathcal{G}} \overline{\alpha}_{ijk} \left(\rho_{ij}(k) - \sum_n x_i[n+k]\overline{h}_j[n]\right)\right] \\
+\mathrm{Re}\left[\sum_{i,n} \overline{\beta}_{in} (x_i[n] - y_i[n])\right] + \frac{\theta_1}{2}\left(\sum_i \left|\mathbf{h}_i^H \mathbf{x}_i - N\right|^2\right) \\
+\frac{\theta_2}{2}\left(\sum_{(i,j,k)\in(\cup_{g=1}^{G}\mathcal{K}_g)\cup\mathcal{G}} \left|\rho_{ij}(k) - \sum_n x_i[n+k]\overline{h}_j[n]\right|^2\right) \\
+\frac{\theta_3}{2}\left(\sum_{i,n} |x_i[n] - y_i[n]|^2\right)
\end{array}
\tag{15}
$$

where $\mathrm{Re}[\cdot]$ represents the real part of a complex number. θ_1, θ_2, and θ_3 are penalty parameters. $\{\lambda_i\}$, $\{\alpha_{ijk}\}$, and $\{\beta_{in}\}$ are Lagrangian multipliers, also dual variables. To solve problem (14), we propose a group orthogonal waveform design algorithm based on a primal-dual type method. The proposed algorithm decomposes problem (14) into a series of simple subproblems. By sequentially updating the optimization variables and dual variables, the proposed algorithm minimizes the augmented Lagrange function L in Equation (15) after several iterations. According to optimization model (13), the variables $\left\{\mathbf{x}_i^{(l)}\right\}_{i=1}^{GM}$, $\{\mathbf{y}_i\}_{i=1}^{GM}$, and $\left\{\mathbf{h}_i^{(l)}\right\}_{i=1}^{GM}$ converge to the same point. The convergence condition is $\sum_i \|\mathbf{h}_i^{(l)} - \mathbf{x}_i^{(l)}\|_2^2 / \sum_i \|\mathbf{x}_i^{(l)}\|_2^2 < \eta$. Algorithm 1 summarizes the proposed algorithm. The subproblems of the proposed group orthogonal waveform design algorithm can be expressed as follows:

$$
\mathcal{P}_1 : \left\{ \underset{\substack{|\rho_{ij}(k)|\le\varepsilon_g,\ \forall(i,j,k)\in\mathcal{K}_g,\ g=1,2,\ldots,G \\ |\rho_{ij}(k)|\le\gamma,\ \forall(i,j,k)\in\mathcal{G}}}{\varepsilon_1, \cdots, \varepsilon_G, \gamma, \ \ \rho_{ij}(k)\}^{(l+1)}} = \arg\min L \begin{pmatrix} \varepsilon_1, \cdots, \varepsilon_G, \gamma, \rho_{ij}(k) \\ \left\{\mathbf{x}_i, \mathbf{y}_i, \mathbf{h}_i, \lambda_i, \alpha_{ijk}, \beta_{in}\right\}^{(l)} \end{pmatrix} \right.
\tag{16}
$$

$$\mathcal{P}_2 : \left\{ \{\mathbf{h}_i\}^{(l+1)} = \underset{\|\mathrm{h}_i\|_2^2 \le N, \forall i}{\operatorname{argmin}} \; L\left(\begin{array}{c} \{\varepsilon_1, \cdots, \varepsilon_G, \gamma, \rho_{ij}(k)\}^{(l+1)}, \\ \{\mathbf{h}_i\}, \left\{\mathbf{x}_i, \mathbf{y}_i, \lambda_i, \alpha_{ijk}, \beta_{in}\right\}^{(l)} \end{array} \right) \right. \tag{17}$$

$$\mathcal{P}_3 : \left\{ \{\mathbf{x}_i\}^{(l+1)} = \operatorname{argmin} L(\ldots, \{\mathbf{x}_i\}, \ldots) \right. \tag{18}$$

$$\mathcal{P}_4 : \left\{ \{\mathbf{y}_i\}^{(l+1)} = \underset{|y_i[n]|=1, \forall (i,n)}{\operatorname{argmin}} \; L(\ldots, \{\mathbf{y}_i\}, \ldots) \right. \tag{19}$$

$$\left\{ \begin{array}{l} \lambda_i^{(l+1)} = \lambda_i^{(l)} + c\theta_1\left(\left(\mathbf{h}_i^{(l+1)}\right)^H \mathbf{x}_i^{(l+1)} - N \right) \\ \alpha_{ijk}^{(l+1)} = \alpha_{ijk}^{(l)} + c\theta_2\left(\rho_{ij}^{(l+1)}(k) - \sum_n x_i^{(l+1)}[n+k]\overline{h}_j^{(l+1)}[n] \right) \\ \beta_{in}^{(l+1)} = \beta_{in}^{(l)} + c\theta_3\left(x_i^{(l+1)}[n] - y_i^{(l+1)}[n] \right) \end{array} \right. \tag{20}$$

Parameter c in Equation (20) is the step length. Superscript (l) represents the values of the variables at the l-th iteration. Except for subproblem $\mathcal{P}_1$, subproblems $\mathcal{P}_2$, $\mathcal{P}_3$, and $\mathcal{P}_4$ are actually the same as the primal-dual algorithm [18], and can be solved using similar methods to primal-dual. In the remainder of this section, methods to solve these subproblems are introduced.

Algorithm 1 Group Orthogonal Waveform Design Algorithm

Initialization

Randomly select $\left\{\mathbf{x}_i^{(0)}\right\}_{i=1}^{GM}$ (constant modulus is not required).

Set constant modulus $\left\{\mathbf{y}_i^{(0)}\right\}_{i=1}^{GM}$ using the phases of $\left\{\mathbf{x}_i^{(0)}\right\}_{i=1}^{GM}$.

Randomly select $\{\lambda_i\}$, $\{\alpha_{ijk}\}$, $\{\beta_{in}\}$ and $\left\{\mathbf{h}_i^{(0)}\right\}_{i=1}^{GM}$, set $l = 0$.

Repeat

Compute $\left\{\varepsilon_1, \cdots, \varepsilon_G, \gamma, \rho_{ij}(k)\right\}^{(l+1)}$ by solving subproblem (16).

Compute $\{\mathbf{h}_i\}^{(l+1)}$ by solving subproblem (17).

Compute $\{\mathbf{x}_i\}^{(l+1)}$ by solving subproblem (18).

Compute $\{\mathbf{y}_i\}^{(l+1)}$ by solving subproblem (19).

Compute $\lambda_i^{(l+1)}, \alpha_{ijk}^{(l+1)}, \beta_{in}^{(l+1)}$ using (20), $l = l + 1$.

Until $\sum_i \|\mathbf{h}_i^{(l)} - \mathbf{x}_i^{(l)}\|_2^2 / \sum_i \|\mathbf{x}_i^{(l)}\|_2^2 < \eta$.

3.1. Solving Subproblem $\mathcal{P}_1$

According to the augmented Lagrange function (15), subproblem (16) can be separated into two independent parts as follows:

$$\begin{array}{c} \min\limits_{|\rho_{ij}(k)| \le \varepsilon_g} w\varepsilon_g^2/G + \sum\limits_{(i,j,k) \in \mathcal{K}_g} \left[a_{ijk}\left|\rho_{ij}(k)\right|^2 + \mathrm{Re}\left(\overline{b}_{ijk}\rho_{ij}(k)\right) \right] \\ g = 1, 2, \ldots, G \end{array} \tag{21}$$

$$\min_{|\rho_{ij}(k)| \le \gamma} (1-w)\gamma^2 + \sum_{(i,j,k) \in \mathcal{G}} \left[a_{ijk}\left|\rho_{ij}(k)\right|^2 + \mathrm{Re}\left(\overline{b}_{ijk}\rho_{ij}(k)\right) \right] \tag{22}$$

where $a_{ijk} = \theta_2/2,\ b_{ijk} = \alpha_{ijk}^{(l)} - \theta_2 \cdot \sum_n x_i^{(l)}[n+k]\overline{h}_j^{(l)}[n]$. Considering problem (21), when ε_g is fixed, the optimal solution of $\rho_{ij}(k)$ for every index (i,j,k) can be expressed as

$$\rho_{ijk}^*(\varepsilon_g) = \left\{ \begin{array}{l} -b_{ijk}/\left(2a_{ijk}\right), \left|b_{ijk}/\left(2a_{ijk}\right)\right| \le \varepsilon_g \\ -\left(b_{ijk}/\left|b_{ijk}\right|\right)\varepsilon_g, \text{ others} \end{array} \right. \tag{23}$$

where $\rho^*_{ijk}(\varepsilon_g)$ is a function of ε_g. According to Equation (23), problem (21) is equivalent to

$$\min_{\varepsilon_g \geq 0} f(\varepsilon_g) \triangleq w\varepsilon_g^2/G + \sum_{(i,j,k)\in\mathcal{K}_g} f^*_{ijk}(\varepsilon_g),\ g = 1, 2, \ldots, G \tag{24}$$

where

$$\begin{aligned} f^*_{ijk}(\varepsilon_g) &= a_{ijk}\left|\rho^*_{ijk}(\varepsilon_g)\right|^2 + \mathrm{Re}\left(\bar{b}_{ijk}\rho^*_{ijk}(\varepsilon_g)\right) \\ &= \begin{cases} -\left|b_{ijk}\right|^2/\left(4a_{ijk}\right), \left|b_{ijk}/\left(2a_{ijk}\right)\right| \leq \varepsilon_g \\ a_{ijk}\varepsilon_g^2 - \left|b_{ijk}\right|\varepsilon_g, \text{ others} \end{cases} \end{aligned} \tag{25}$$

Because $f(\varepsilon_g) \leq f(-\varepsilon_g)$, the condition $\varepsilon_g \geq 0$ can be ignored. The optimal ε^*_g value can be determined by solving the following equation:

$$\nabla f(\varepsilon_g) = 2w\varepsilon_g + \sum_{(i,j,k)\in\mathcal{K}_g} \min\left\{2a_{ijk}\varepsilon_g - \left|b_{ijk}\right|, 0\right\} = 0 \tag{26}$$

Because $a_{ijk} = \theta_2/2 > 0$, $\nabla f(\varepsilon_g)$ is a monotonically increasing function of ε_g. The optimal $\varepsilon_g^{(l+1)} = \varepsilon^*_g$ value can be obtained efficiently via the bisection method. Similarly, the optimal solution $\gamma^{(l+1)} = \gamma^*$ of problem (22) can be obtained by solving the following equation:

$$2(1-w)\gamma + \sum_{(i,j,k)\in\mathcal{G}} \min\left\{2a_{ijk}\gamma - \left|b_{ijk}\right|, 0\right\} = 0 \tag{27}$$

3.2. Solving Subproblem $\mathcal{P}_2$

According to Equation (15), subproblem (17) is separable for each $\mathbf{h}_i$, i = 1, 2,..., GM. The minimization problem can be expressed as follows:

$$\min_{\|\mathbf{h}_i\|_2^2 < N} f(\mathbf{h}_i) \triangleq \mathbf{h}_i^H \mathbf{A}_i \mathbf{h}_i + \mathrm{Re}\left(\mathbf{t}_i^H \mathbf{h}_i\right) \tag{28}$$

where

$$\mathbf{A}_i = (\theta_2/2) \cdot \textstyle\sum_{j,k} \mathbf{x}^{(l)}_{j,(-k)} \mathbf{x}^{(l)H}_{j,(-k)} \tag{29}$$

$$\mathbf{t}_i = \overline{\lambda}_i^{(l)} \mathbf{x}_i^{(l)} - \theta_1 N \mathbf{x}_i^{(l)} - \textstyle\sum_{j,k} \left(\overline{\alpha}^{(l)}_{jik} + \theta_2 \overline{\rho}^{(l+1)}_{ji}(k)\right) \mathbf{x}^{(l)}_{j,(-k)} \tag{30}$$

where $\mathbf{x}_{j,k}$ represents the aperiodic delayed copy of the discrete signal $\mathbf{x}_j$. For $k \geq 0$, $\mathbf{x}_{j,k} = (x_j[k+1], x_j[k+2], \cdots, x_j[N], \mathbf{0}_{1\times k})^{\mathrm{T}}$; for $k \leq 0$, $\mathbf{x}_{j,k} = (\mathbf{0}_{1\times|k|}, x_j[1], x_j[2], \cdots, x_j[N-|k|])^{\mathrm{T}}$. The augmented Lagrange function of problem (28) can be expressed as follows:

$$L_i(\mathbf{h}_i, \lambda) = \mathbf{h}_i^H \mathbf{A}_i \mathbf{h}_i + \mathrm{Re}\left(\mathbf{t}_i^H \mathbf{h}_i\right) + \lambda\left(\|\mathbf{h}_i\|_2^2 - N\right) \tag{31}$$

The Karush–Kuhn–Tucker (KKT) conditions for problem (28) are as follows:

$$\begin{cases} \|\mathbf{h}^*_i\|_2^2 \leq N, \quad 2\mathbf{A}_i\mathbf{h}^*_i + \mathbf{t}_i + 2\lambda^*\mathbf{h}^*_i = 0 \\ \lambda^* \geq 0, \quad \lambda^*\left(\|\mathbf{h}^*_i\|_2^2 - N\right) = 0 \end{cases} \tag{32}$$

Obviously, when $\lambda^* = 0$, KKT condition (32) is equivalent to

$$\|\mathbf{h}^*_i\|_2^2 \leq N,\ \mathbf{h}^*_i = -\mathbf{A}_i^{-1}\mathbf{t}_i/2 \tag{33}$$

If condition (33) is true, then $\mathbf{h}_i^{(l+1)} = \mathbf{h}^*_i$; otherwise, the optimal solution should found under the condition of $\lambda^* > 0$.

When $\lambda^* > 0$, condition (32) is equivalent to

$$\|\mathbf{h}_i^*\|_2^2 = N, \mathbf{h}_i^* = -(\mathbf{A}_i + 2\lambda^*\mathbf{I})^{-1}\mathbf{t}_i/2 \tag{34}$$

In order to solve Equation (34), the value of λ^* should be determined. According to Equation (31), for any fixed value of $\lambda > 0$, the optimal $\mathbf{v}(\lambda)$ with minimal $L_i(\mathbf{v}(\lambda), \lambda)$ is below.

$$\mathbf{v}(\lambda) = -(\mathbf{A}_i + 2\lambda\mathbf{I})^{-1}\mathbf{t}_i/2 \tag{35}$$

If $0 < \lambda' < \lambda$, then

$$\begin{cases} L_i(\mathbf{v}(\lambda), \lambda) \leq L_i(\mathbf{v}(\lambda'), \lambda) \\ L_i(\mathbf{v}(\lambda'), \lambda') \leq L_i(\mathbf{v}(\lambda), \lambda') \end{cases} \tag{36}$$

According to function (31), and after summing the two inequalities in (36), then

$$(\lambda' - \lambda)\|\mathbf{v}(\lambda')\|_2^2 \leq (\lambda' - \lambda)\|\mathbf{v}(\lambda)\|_2^2 \tag{37}$$

Therefore, $\|\mathbf{v}(\lambda)\|_2^2$ is a monotone decreasing function of λ. Solving the KKT conditions when $\lambda^* > 0$ is equivalent to finding the zero of function $\|\mathbf{v}(\lambda)\|_2^2 - N$, which can be achieved via the bisection method.

3.3. Solving Subproblem $\mathcal{P}_3$

According to Equation (15), subproblem (18) can be separated into the following unconstrained convex problem for each $\mathbf{x}_i$, $i = 1, 2, \ldots, GM$:

$$\min_{\mathbf{x}_i} f(\mathbf{h}_i) \triangleq \mathbf{x}_i^H \mathbf{C}_i \mathbf{x}_i + \mathrm{Re}\left(\mathbf{d}_i^H \mathbf{x}_i\right) \tag{38}$$

where

$$\mathbf{C}_i = (\theta_2/2) \cdot \sum\nolimits_{j,k} \mathbf{h}_{j,k}^{(l+1)} \mathbf{h}_{j,k}^{(l+1)H} + (\theta_3/2)\mathbf{I} \tag{39}$$

$$\mathbf{d}_i = \lambda_i^{(l)} \mathbf{h}_i^{(l+1)} + \boldsymbol{\beta}_i^{(l)} - \theta_1 N \mathbf{h}_i^{(l+1)} - \sum\nolimits_{j,k} \left(\alpha_{ijk}^{(l)} + \theta_2 \rho_{ij}^{(l+1)}(k)\right) \mathbf{h}_{j,k}^{(l+1)} - \theta_3 \mathbf{y}_i^{(l)} \tag{40}$$

where $\mathbf{h}_{j,k}$ represents the periodic delayed copy of $\mathbf{h}_j$, similar to $\mathbf{x}_{j,k}$ in Equations (29) and (30). It is easy to determine that $\mathbf{C}_i$ in Equation (39) is an $N \times N$ positive definite matrix. Therefore, subproblem (38) is an unconstrained quadratic optimization problem, the optimal solution of which is $\mathbf{x}_i^{(l+1)} = \mathbf{x}_i^* = -\mathbf{C}_i^{-1}\mathbf{d}_i/2$, which can be found efficiently via conjugate gradient methods.

3.4. Solving Subproblem $\mathcal{P}_4$

According to Equation (15), subproblem (19) can be separated for each $y_i[n]$, $i = 1, 2, \ldots, GM$, $n = 1, 2, \ldots, N$, as follows:

$$\min_{|y_i[n]|=1} \mathrm{Re}[\overline{u}_{in} y_i[n]] \tag{41}$$

where

$$u_{in} = -\beta_{in}^{(l)} - \theta_3 x_i^{(l+1)}[n] \tag{42}$$

Define $\overline{u}_{in} = |\overline{u}_{in}| \cdot \exp(\mathrm{j}\phi_{in})$. Then, the solution of subproblem (41) can be expressed as $y_i^{(l+1)}[n] = y_i^*[n] = \exp(\mathrm{j} \cdot (\pi - \phi_{in}))$.

4. Numerical Results

In order to demonstrate the effectiveness of Algorithm 1, in this section, a series of numerical simulations is shown. The parameters are initialized as $c = 0.5$, $\theta_1 = \theta_2 = 10$. The parameter is set as $\theta_3 = \max\{10, \min\{2(l+1), 10^5\}\}$, where l is the current iteration. The parameter of the convergence condition is $\eta = 0.5 \times 10^{-3}$. All experiments were implemented in MATLAB 2020a on a PC with one Intel Core i7-7700 CPU and 16 GB RAM.

All the obtained correlation function values and PSL and PCL metrics in dB were calculated as $10\log_{10}(|r_{ij}(k)|^2/N^2)$.

4.1. Effect of Weighting Factor *w*

Figure 1 shows the convergence curves of the variables γ and ε_g, $g = 1, 2, \ldots, G$ with different parameters. The computational complexity per iteration of the proposed algorithm is $\mathcal{O}(MGN^2 + M^2G^2N\log N)$. The algorithm running time with $M = 2$, $G = 2$, and $N = 256$ is around 700 s on average. The convergence curves of the variables γ and ε_g are not monotonically decreasing because the proposed algorithm minimizes the augmented Lagrange function L in Equation (15). When the convergence condition is satisfied, the variables $\left\{\mathbf{x}_i^{(l)}\right\}_{i=1}^{GM}$ and $\left\{\mathbf{h}_i^{(l)}\right\}_{i=1}^{GM}$ are almost the same, and the correlation function $r_{ij}(k)$ satisfies $r_{ij}(k) = \rho_{ij}(k)$. Thus, PCL, PSL_1, $\mathrm{PSL}_2, \ldots, \mathrm{PSL}_G$ are minimized effectively with the help of the auxiliary variables.

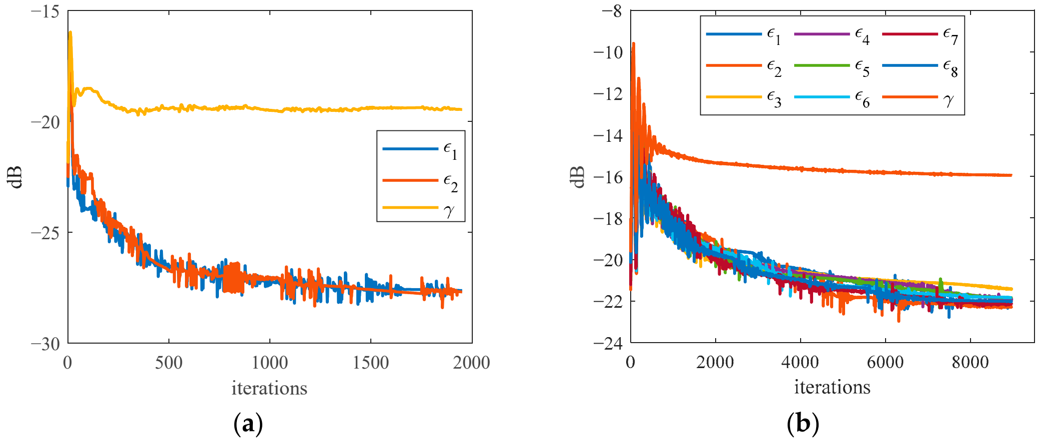

Figure 1. The convergence curves of γ and ε_g, $g = 1,2,\ldots,G$. (**a**) $w = 0.1$, $M = 2$, $G = 2$, $N = 256$; (**b**) $w = 0.7$, $M = 8$, $G = 8$, $N = 256$.

Figure 2a shows the PSL_1, PSL_2, and PCL values obtained with different values of w, with fixed parameters of $M = 2$, $G = 2$, and $N = 256$. Figure 2b shows similar results with $M = 8$, $G = 8$, and $N = 256$. The maximum and minimum values of PSL_1, $\mathrm{PSL}_2, \ldots, \mathrm{PSL}_G$ are shown, denoted by $\mathrm{PSL}_{\max}$ and $\mathrm{PSL}_{\min}$, respectively. It can be seen that the smaller the value of w, the lower the obtained intragroup PSL values and the higher the obtained intergroup PCL value. The results in Figure 2 demonstrate that the proposed algorithm is able to adjust the weighting factor w to balance the intra- and intergroup correlation performances, which is suitable for different MIMO radar applications.

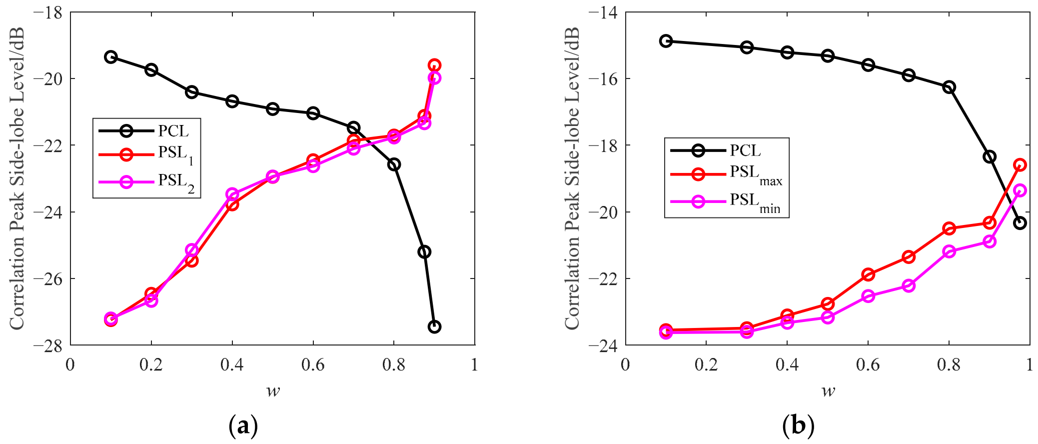

Figure 2. The convergence curves of γ and ε_g, $g = 1,2,\ldots,G$. (**a**) $M = 2$, $G = 2$, $N = 256$; (**b**) $M = 8$, $G = 8$, $N = 256$.

4.2. Obtained Correlation Functions

In his subsection, plots of the intra- and intergroup correlation function curves are detailed. The waveforms obtained by the proposed group orthogonal waveform algorithm are compared to other advanced orthogonal waveforms under different parameters. In Figure 3, random set represents the waveforms generated directly by random numbers. Multi-CAN is one of the best ISL minimization algorithms, and the primal-dual and p-MM algorithms are the current best PSL optimization algorithms. The up- and down-chirp signals have the lowest cross-correlation function when $M = 2$. Therefore, by setting the same time-bandwidth product equal to $N = 256$, the up- and down-chirp signals can be compared to the intragroup orthogonal performance of the waveforms when $M = 2$.

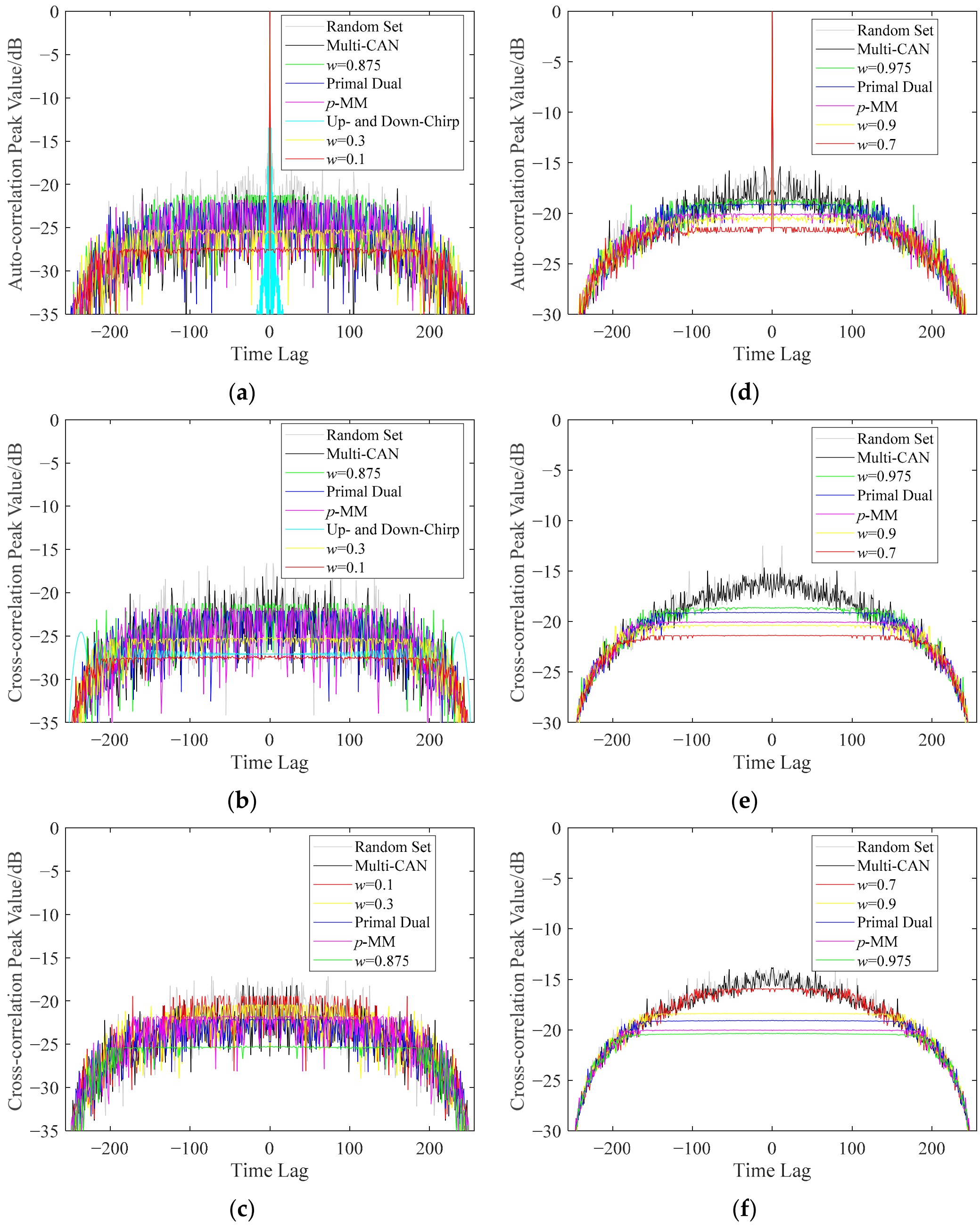

Figure 3. The correlation peak value obtained by the proposed algorithm when $M = 2$, $G = 2$, and $N = 256$: (**a**) autocorrelation; (**b**) intragroup cross-correlation; (**c**) intergroup cross-correlation, and when $M = 8$, $G = 8$, and $N = 256$: (**d**) autocorrelation; (**e**) intragroup cross-correlation; (**f**) intergroup cross-correlation.

Figure 3a shows the autocorrelation function peak value of the GM waveforms when $M = 2$, $G = 2$, and $N = 256$. Figure 3b shows the intragroup cross-correlation function peak value, while Figure 3c shows the intergroup cross-correlation function peak value. When $w = 0.1$, the intragroup correlation side-lobe peak value obtained by the proposed algorithm is the lowest in comparison to other waveforms with relatively higher intergroup cross-correlation function peak values. When $w = 0.875$, although the intragroup auto- and cross-correlation functions of the waveforms obtained by the proposed algorithm are relatively high, the intergroup cross-correlation functions are the lowest. The results when $w = 0.3$ lie between those when $w = 0.1$ and $w = 0.875$. Figure 3d–f show the results when $M = 8$, $G = 8$, and $N = 256$.

The results in Figure 3 demonstrate that, with typical parameter values, the proposed group orthogonal waveform design algorithm is able to effectively balance the intra- and intergroup correlation function performances. To briefly summarize, compared with designing all the GM waveforms directly, as performed in the primal-dual algorithm, the proposed group orthogonal waveform design algorithm is able to obtain lower intragroup PSL metrics by sacrificing a small portion of the intergroup cross-correlation performance and vice versa. Therefore, for antijamming agile waveform applications, the proposed algorithm is more flexible. The proposed group orthogonal waveform design algorithm is able to design multiple groups of orthogonal waveform sets at the same time.

4.3. Effect of M, N, G Parameters

In Figure 4a,b, the effect of the phase coding sequence length N on the results is analyzed. In the simulations, the weighting factor w and the waveform parameters $M = 2$, $G = 2$ were unchanged. The waveforms were obtained by the proposed algorithm with $N = 32, 64, 96, 128, 160, 192, 224$, and 256. After calculating the PCL and intragroup PSL metrics (the PSL metrics are denoted as PSL_1 and PSL_2 because $G = 2$), Figure 4a,b show the obtained metric values when $w = 0.3$ and $w = 0.875$, respectively. The results demonstrate that the larger the sequence length, the lower the obtained PCL and PSL values.

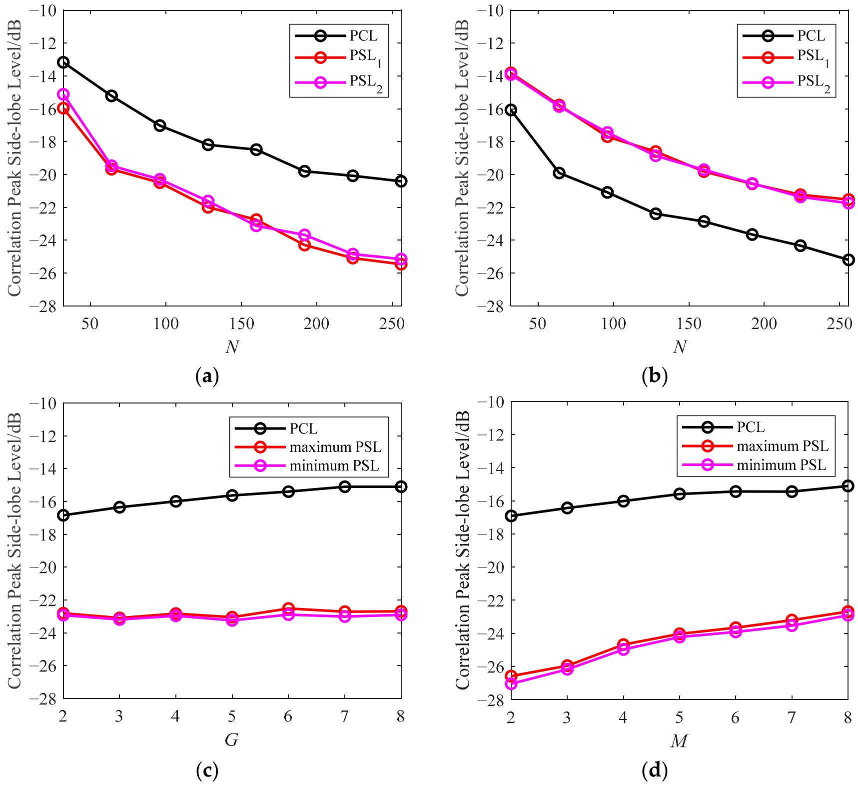

Figure 4. The effect of parameters M, N, and G on the obtained metric values. (**a**) $w = 0.3$, $M = 2$, $G = 2$; (**b**) $w = 0.875$, $M = 2$, $G = 2$; (**c**) $w = 0.5$, $M = 8$, $N = 256$; (**d**) $w = 0.5$, $G = 8$, $N = 256$.

In Figure 4c,d, the effects of the number of groups G and the number of intragroup waveforms M on the results are analyzed. Firstly, the weighting factor was set to $w = 0.5$ and the parameters were set to $M = 8$, $N = 256$. Then, the proposed algorithm was used to obtain the waveforms at $G = 2, 3, 4, 5, 6, 7$, and 8. Finally, the PCL metric value was calculated as well as the maximum and minimum values of PSL_1, $\mathrm{PSL}_2, \ldots, \mathrm{PSL}_G$. The results are shown in Figure 4c. It can be seen that the PCL increases with an increase in G, because the total number of waveforms, GM, increases. Meanwhile, the obtained intragroup PSL values change little with an increase in G, because the number of intragroup waveforms $M = 8$ remains unchanged. In Figure 4d, the parameter $G = 8$ is unchanged and the proposed algorithm is initiated with $M = 2, 3, 4, 5, 6, 7$, and 8. It can be seen that the intragroup PSL metric values increase with an increase in M. Overall, the PCL metric value mainly depends on the total number of waveforms GM. The intragroup PSL metric values mainly depend on the parameter M.

4.4. Antijamming Simulation

In this section, the jamming suppression performances of MIMO radar using the different waveforms in Table 1 are analyzed. The transmitted phase-coded pulse signal generated using the group orthogonal waveforms $\{\mathbf{x}_i\}_{i=1}^{GM}$ can be expressed as follows:

$$x_i(t) = \exp(\mathrm{j}2\pi\frac{\mathrm{c}}{\lambda}t) \cdot \sum_{n=0}^{N-1} p_\tau(t - n\tau)x_i[n],\ i = 1, 2, \ldots, GM,\ p_\tau(t) = \begin{cases} 1, 0 < t \leq \tau \\ 0,\ \text{others} \end{cases} \tag{43}$$

where c is the speed of light, τ is the chip length, and λ is the carrier wavelength. There are N_t transmitting elements and N_r receiving elements; the digital signal after matched filtering can be expressed as $\mathbf{y}[n] = (y_1[n], \ldots, y_{N_t N_r}[n])^{\mathrm{T}}$. Then, the digital beam forming output is equal to

$$\mathbf{I}(\theta, n) = \left[\mathbf{a}_r(\theta) \otimes \mathbf{a}_t^{\mathrm{H}}(\theta)\right]^{\mathrm{H}} \mathbf{y}[n] \tag{44}$$

where $\mathbf{I}$ is the angle–range image. $\mathbf{a}_t(\theta) = (1, \exp(-\mathrm{j}\alpha_t), \exp(-\mathrm{j}2\alpha_t), \ldots, \exp(-\mathrm{j}(N_t - 1)\alpha_t))^{\mathrm{T}}$ is the transmit steering vector and $\mathbf{a}_r(\theta) = (1, \exp(-\mathrm{j}\alpha_r), \exp(-\mathrm{j}2\alpha_r), \ldots, \exp(-\mathrm{j}(N_r - 1)\alpha_r))^{\mathrm{T}}$ is the receive steering vector, with $\alpha_t = 2\pi \sin\theta d_t/\lambda$ and $\alpha_r = 2\pi \sin\theta d_r/\lambda$. The uniform linear array consists of $N_t = 3$ transmit elements spaced at $d_t = 16\lambda$ apart, and $N_r = 16$ receive elements spaced at $d_r = 0.5\lambda$ apart. $\otimes$ represents the Kronecker product and θ represents the direction of arrival. Figure 5 shows a block diagram of the processing in the simulation. The size of range bins is 100 m. The range corresponding to the first bin is 50 km. The angles, ranges, and signal-to-noise ratios of the four true targets are $(-15°, 400, 3\ \mathrm{dB})$, $(0°, 400, 3\ \mathrm{dB})$, $(20°, 400, 3\ \mathrm{dB})$, and $(20°, 50, 5\ \mathrm{dB})$, respectively, where the range parameters' units are range bins. DRFM-based deceptive jamming causes two false targets, whose angles, ranges, and jamming-to-noise ratios are $(-15°, 50, 5\ \mathrm{dB})$ and $(0°, 50, 5\ \mathrm{dB})$, respectively. The noise is Gaussian random white noise.

Table 1. Parameters and performance metrics of simulated waveforms.

Waveform Design Method	Title 2	Title 3
Fixed waveform	$M = 3$, $N = 256$	PSL = −23.22 dB
Multi-CAN [12]	$MG = 6$, $N = 256$	PSL = −17.02 dB
Primal-dual [18]	$MG = 6$, $N = 256$	PSL = −20.18 dB
p-MM [19]	$MG = 6$, $N = 256$	PSL = −20.42 dB
Proposed method when $w = 0.9$	$M = 3$, $G = 2$, $N = 256$	$\mathrm{PSL}_1 = -19.18$ dB
		$\mathrm{PSL}_2 = -19.39$ dB
		PCL = −25.56 dB
Proposed method when $w = 0.1$	$M = 3$, $G = 2$, $N = 256$	$\mathrm{PSL}_1 = -25.64$ dB
		$\mathrm{PSL}_2 = -25.88$ dB
		PCL = −18.51 dB

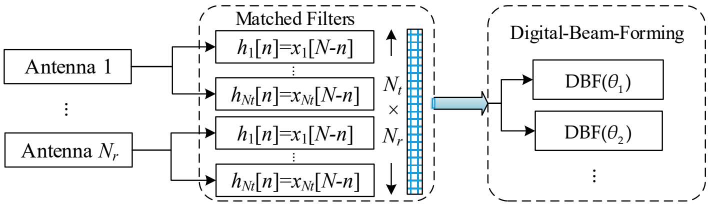

Figure 5. The block diagram of the matched filtering and digital beam forming processes.

Assuming that one pulse of the waveform has been intercepted, Figure 6 shows the angle–range images formed with MIMO radar using adjacent pulse echoes. The results show that the proposed algorithm is able to balance the antijamming and range compression performances by adjusting the weighing factor. On this basis, the waveform diversity gain of MIMO radar can be maximized by selecting a proper waveform set as the best response to flexible adaptive deceptive jamming [26].

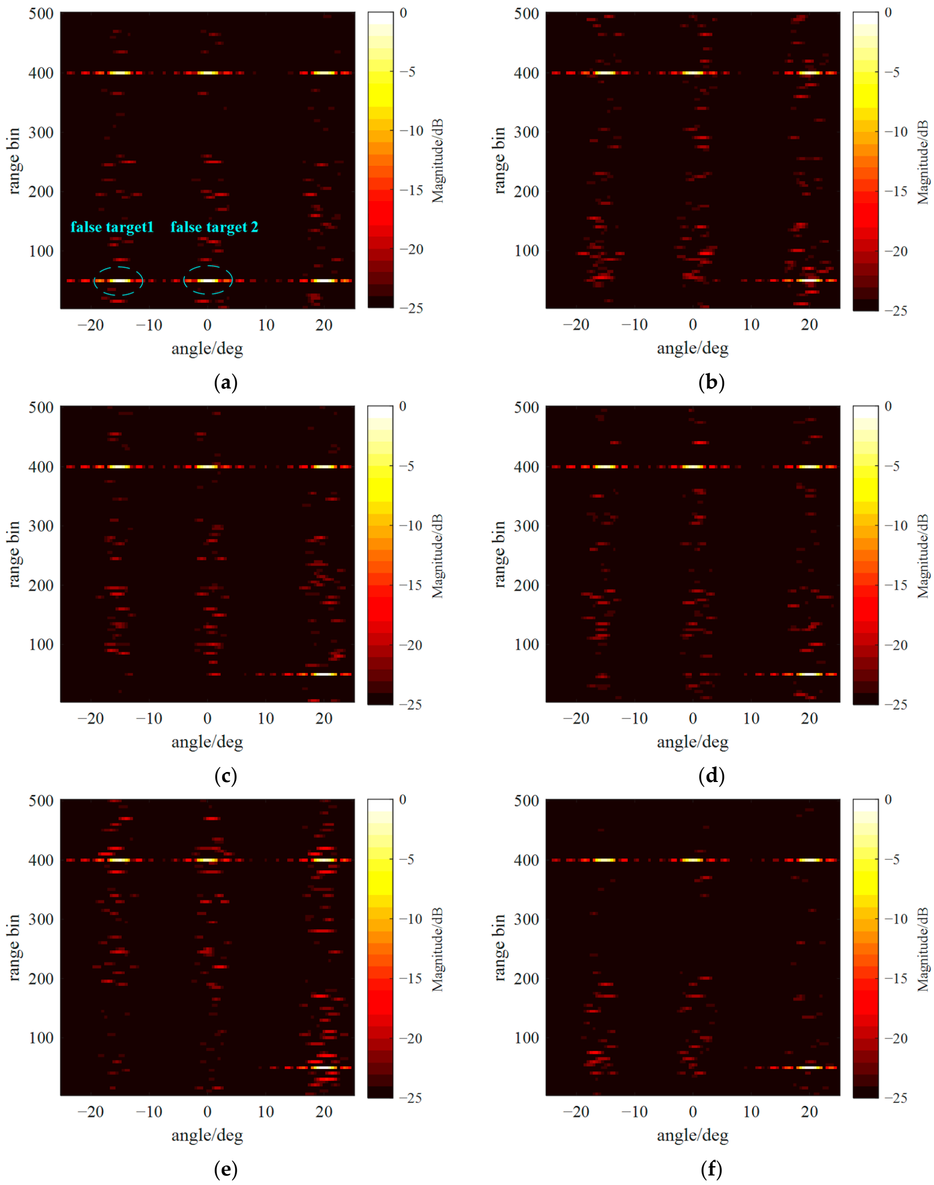

Figure 6. Angle–range images formed with MIMO radar using fixed and agile waveforms under DRFM-based deceptive jamming. (**a**) Fixed waveform; (**b**) primal-dual; (**c**) Multi-CAN; (**d**) p-MM; (**e**) $w = 0.9$, $M = 3$, $G = 2$, $N = 256$; (**f**) $w = 0.1$, $M = 3$, $G = 2$, $N = 256$.

5. Conclusions

Transmitting agile group orthogonal waveforms is an effective way for MIMO radar to combat DRFM jamming. Aiming at balancing the waveform diversity gain and jamming suppression performance for an MIMO radar system, in this article, a group orthogonal waveform optimal design model was proposed. The objective function separates the waveform performances into two parts. The first part is the peak value of intragroup auto- and cross-correlation functions. The other part is the peak value of the intergroup cross-correlation functions. To solve the proposed optimization problem, after proper relaxations, in this article, a group orthogonal waveform design algorithm was proposed, transforming the minimization of the augmented Lagrange function into a series of subproblems. The numerical results showed that the proposed algorithm can minimize the intra- and intergroup correlation functions effectively. The antijamming simulation results showed that the proposed algorithm is able to achieve a balance between the DRFM-based deceptive jamming suppression and range compression performances. The proposed algorithm is flexible and has potential in adaptive antijamming applications for MIMO radars.

Author Contributions: Conceptualization, T.L. and J.S.; methodology, T.L.; software, T.L.; validation, J.S., G.W., X.Y. and Y.Q.; formal analysis, T.L.; investigation, T.L.; resources, J.S.; data curation, T.L.; writing—original draft preparation, T.L.; writing—review and editing, J.S., G.W., X.Y. and Y.Q.; visualization, T.L.; supervision, J.S.; project administration, X.Y.; funding acquisition, J.S. All authors have read and agreed to the published version of the manuscript.

Funding: This work was supported in part by National Natural Science Foundation of China under grant 62131001 and grant 62171029, Key R&D Plan of Zhejiang Province (2023C01148) and the Hangzhou Leading Innovation and Entrepreneurship Team (TD2022006).

Data Availability Statement: The data will be made available by the authors on request.

Conflicts of Interest: Guohua Wang was employed by Hertzwell Pte Ltd. The remaining authors declare that the research was conducted in the absence of any commercial or financial relationships that could be construed as a potential conflict of interest. Hertzwell Pte Ltd. had no role in the design of the study; in the collection, analyses, or interpretation of data; in the writing of the manuscript, or in the decision to publish the results.

References

1. Li, J.; Stoica, P. MIMO Radar with Colocated Antennas. *IEEE Signal Process. Mag.* **2007**, *24*, 106–114. [CrossRef]
2. Fishler, E.; Haimovich, A.; Blum, R.S.; Cimini, L.J.; Chizhik, D.; Valenzuela, R.A. Spatial Diversity in Radars—Models and Detection Performance. *IEEE Trans. Signal Process.* **2006**, *54*, 823–838. [CrossRef]
3. Haimovich, A.M.; Blum, R.S.; Cimini, L.J. MIMO Radar with Widely Separated Antennas. *IEEE Signal Process. Mag.* **2008**, *25*, 116–129. [CrossRef]
4. Bergin, J.; Guerci, J.R. *MIMO Radar: Theory and Application*; Artech House: Boston, MA, USA, 2018; pp. 45–49.
5. Friedlander, B. Waveform Design for MIMO Radars. *IEEE Trans. Aerosp. Electron. Syst.* **2007**, *43*, 1227–1238. [CrossRef]
6. Kajenski, P.J. Design of Low-Sidelobe Phase-Coded Waveforms. *IEEE Trans. Aerosp. Electron. Syst.* **2019**, *55*, 2891–2898. [CrossRef]
7. Hassan, A.K.; Al-Saggaf, U.M.; Moinuddin, M.; Alshoubaki, M.K. Statistical Method Based Waveform Optimization in Collocated MIMO Radar Systems. *Mathematics* **2023**, *11*, 680. [CrossRef]
8. Pace, P. *Detecting and Classifying Low Probability of Intercept Radar*, 2nd ed.; Artech House: Boston, MA, USA, 2008; pp. 358–377.
9. Keel, B.M.; Baden, J.M.; Heath, T.H. A Comprehensive Review of Quasi-Orthogonal Waveforms. In Proceedings of the 2007 IEEE Radar Conference, Waltham, MA, USA, 17–20 April 2007.
10. Liu, H.; Zhou, S.; Zang, H.; Cao, Y. Two Waveform Design Criteria for Colocated MIMO Radar. In Proceedings of the 2014 International Radar Conference, Lille, France, 13–17 October 2014.
11. Gini, F.; Maio, A.D.; Patton, L. *Waveform Design and Diversity for Advanced Radar Systems*; IET: London, UK, 2012; pp. 89–117.
12. He, H.; Stoica, P.; Li, J. Designing Unimodular Sequence Sets with Good Correlations—Including an Application to MIMO Radar. *IEEE Trans. Signal Process.* **2009**, *57*, 4391–4405. [CrossRef]
13. Song, J.; Babu, P.; Palomar, D.P. Sequence Set Design with Good Correlation Properties via Majorization-Minimization. *IEEE Trans. Signal Process.* **2016**, *64*, 2866–2879. [CrossRef]
14. Li, Y.; Vorobyov, S.A. Fast Algorithms for Designing Unimodular Waveform(s) with Good Correlation Properties. *IEEE Trans. Signal Process.* **2018**, *66*, 1197–1212. [CrossRef]
15. Wang, J.; Wang, Y. Designing Unimodular Sequences with Optimized Auto/Cross-Correlation Properties via Consensus-ADMM/PDMM Approaches. *IEEE Trans. Signal Process.* **2021**, *69*, 2987–2999. [CrossRef]

16. Esmaeili-Najafabadi, H.; Ataei, M.; Sabahi, M.F. Designing Sequence with Minimum PSL Using Chebyshev Distance and its Application for Chaotic MIMO Radar Waveform Design. *IEEE Trans. Signal Process.* **2017**, *65*, 690–704. [CrossRef]
17. Alaee-Kerahroodi, M.; Modarres-Hashemi, M.; Naghsh, M.M. Designing Sets of Binary Sequences for MIMO Radar Systems. *IEEE Trans. Signal Process.* **2019**, *67*, 3347–3360. [CrossRef]
18. Lin, Z.; Pu, W.; Luo, Z.Q. Minimax Design of Constant Modulus MIMO Waveforms for Active Sensing. *IEEE Signal Process. Lett.* **2019**, *26*, 1531–1535. [CrossRef]
19. Liu, T.; Sun, J.; Wang, G.; Du, X.; Hu, W. Designing Low Side-Lobe Level-Phase Coded Waveforms for MIMO Radar Using p-Norm Optimization. *IEEE Trans. Aerosp. Electron. Syst.* **2023**, *59*, 3797–3810. [CrossRef]
20. Hu, J.; Wei, Z.; Li, Y.; Li, H.; Wu, J. Designing Unimodular Waveform(s) for MIMO Radar by Deep Learning Method. *IEEE Trans. Aerosp. Electron. Syst.* **2021**, *57*, 1184–1196. [CrossRef]
21. Feng, D.; Xu, L.; Pan, X.; Wang, X. Jamming Wideband Radar Using Interrupted-Sampling Repeater. *IEEE Trans. Aerosp. Electron. Syst.* **2017**, *53*, 1341–1354. [CrossRef]
22. Pace, P. *Developing Digital RF Memories and Transceiver Technologies for Electromagnetic Warfare*; Artech House: Boston, MA, USA, 2022.
23. Akhtar, J. Orthogonal Block Coded ECCM Schemes against Repeat Radar Jammers. *IEEE Trans. Aerosp. Electron. Syst.* **2009**, *45*, 1218–1226. [CrossRef]
24. Zhang, J.; Xu, N. Discrete Phase Coded Sequence Set Design for Waveform-Agile Radar Based on Alternating Direction Method of Multipliers. *IEEE Trans. Aerosp. Electron. Syst.* **2020**, *56*, 4238–4252. [CrossRef]
25. Boyd, S.; Vandenberghe, L. *Convex Optimization*; Cambridge University Press: Cambridge, UK, 2009; pp. 215–271.
26. Panoui, A.; Lambotharan, S.; Chambers, J.A. Game Theoretic Distributed Waveform Design for Multistatic Radar Networks. *IEEE Trans. Aerosp. Electron. Syst.* **2016**, *52*, 1855–1865. [CrossRef]